



Photocatalytic degradation of Novacron blue and Novacron yellow textile dyes by the TiO₂/palygorskite nanocomposite

Mikaely Lizandra Moreira de Assis¹ · Elmar Damasceno Junior¹ · Janiele Mayara Ferreira de Almeida¹ · Isabel do Nascimento Silva¹ · Rodrigo Victor Barbosa¹ · Lamara Maciel dos Santos¹ · Elizete Faustino Dias¹ · Nedja Suely Fernandes¹ · Carlos Alberto Martinez-Huitle²

Received: 13 January 2021 / Accepted: 15 July 2021 / Published online: 26 July 2021

© The Author(s), under exclusive licence to Springer-Verlag GmbH Germany, part of Springer Nature 2021

Abstract

The photocatalytic discoloration of industrial dyes, Novacron blue (NB) and Novacron yellow (NY), was investigated using composites based on TiO₂ and natural palygorskite (Pal-Ti10 and Pal-Ti30). The method consisted of synthesizing the composites starting from a physical mixture of TiO₂ and natural palygorskite in the presence of alcohol, for impregnation through calcination under conditions of temperature equal to 450 °C and atmospheric air. The characterization techniques used in this work were FTIR, XRD, XRF, SEM, particle size analysis and zeta potential. The photocatalysis for the NB dye was investigated through the application of a factorial 2⁴ experimental design, aiming at the best experimental conditions and finally applying them in another NY industrial dye. The investigated concentrations of NB were 10 ppm and 30 ppm, the composites were synthesized using 10 and 30% (p/p) of titanium dioxide in palygorskite, the two pH values were 2.0 and 6.0 and the light intensities 9 and 18 W were used. Tests performed at pH 2.0, Pal-Ti30 composite, power 18 W and 10 ppm of dye showed 100% color removal of both dyes in 90 min. The bleaching process followed the pseudo-first order kinetic model, and the apparent constants (K_{app}) were 0.0216 min⁻¹ and 0.0193 min⁻¹ for NB and NY dyes, respectively. The results of total organic carbon (TOC) showed mineralization of 61.70% and 58.06% for NB and NY, respectively, in 90 min of treatment, and the by-products were detected by GC-MS.

Keywords Textile dyes · Novacron blue · Novacron yellow · Photocatalysis · Titanium dioxide · Palygorskite

Introduction

One of the biggest environmental problems resulting from industrial activity is the contamination of water resources with waste, providing adverse effects to the ecosystem (Azari et al. 2020). The effluents from the textile industry are one of the greatest examples of vehicles for contamination of aquatic bodies and can consist of substances that remain present in

low concentrations, even after a possible wastewater treatment process. Among these substances are dyes, persistent and highly toxic chemical compounds, difficult to be removed in the conventional treatment process (Bilal et al. 2019).

More than 100,000 synthetic dyes are marketed in order to meet the demands of the various production sectors. However, because they are complex molecules and resistant to degradation and removal, problems arise during their use, causing impacts on the environment and human health (Yagub et al. 2014). It is estimated that about 10 to 15% of industrially used dyes are discarded without undergoing any type of treatment (Silva et al. 2019).

The textile industry is one of the largest generators of industrial waste and has large amounts of dyes, which are often non-biodegradable molecules and have some resistance to some physical-chemical degradation processes. Thus, the lack of an efficient treatment for these residues can promote environmental contamination and cause intense damage to the health of living beings, considering that the presence of color

Responsible Editor: Sami Rtimi

✉ Elmar Damasceno Junior
elmarjunior12@gmail.com

¹ Universidade Federal do Rio Grande do Norte, Instituto de Química, Laboratório de Química Analítica e Meio Ambiente—LAQUAM, Campus Universitário Lagoa Nova, Natal, RN, Brasil

² Universidade Federal do Rio Grande do Norte, Instituto de Química, Laboratório de Eletroquímica Ambiental e Aplicada—LEAA, Campus Universitário Lagoa Nova, Natal, RN, Brasil

in the water causes it to lose its transparency, reducing the permeability of sunlight, affecting the absorption of gases and the balance of the aquatic ecosystem, in addition to the fact that many of these compounds have carcinogenic effects (Rocha et al. 2012; Mishra et al. 2018).

The means of water treatment for human use as well as for returning to aquatic bodies, in most water treatment plants, rely only on conventional processes that consist of the use of methods such as coagulation/flocculation, sedimentation, filtration and disinfection. These methods are not sufficient to promote the removal of some contaminants, such as dyes, and may generate by-products capable of causing damage to the environment and living beings. Avoiding a possible scarcity of water resources has been a major challenge. Therefore, there is a need for more effective methods so that water is treated correctly and returned to nature with excellent quality (Buruga et al. 2019; Queiroz et al. 2019; Azari et al. 2020).

Despite so many studies to achieve the removal of color and by-products from the degradation of dyes, there is still a great concern in having efficient, low-cost and sustainable technologies for this purpose. Among the various effluent treatment methods, advanced oxidative processes (POAs) using photocatalysis have gained prominence for being effective in the process of removing contaminants, in which it is possible to obtain complete oxidation or mineralization of organic compounds at temperature and ambient pressure (Matilainen and Sillanpää 2010; Brillas and Martínez-Huitle 2015).

Novacron blue (NB) and Novacron yellow (NY) are reactive dyes belonging to the group of azo dyes, characterized by the presence of the chromophore group $-N=N-$. Reactive dyes have non-biodegradable molecules and have low adsorption and fixation, making them highly concentrated in effluents, which makes their treatment by conventional methods difficult (Hassan and Carr 2018; Zhang et al. 2020).

The NB dye is commonly used by Brazilian textile industries for dyeing jeans. Such a compound has high hydrophilicity and solubility in saline and alcoholic solutions, and the molecule remains stable when conditioned to an acid or alkaline medium (Rocha et al. 2012; Fernandes Rêgo et al. 2014). NY dye is widely used in the textile industries of north-eastern Brazil. When present in the environment, it affects aquatic ecosystems due to its persistent color, in addition to presenting carcinogenic and mutagenic characteristics (Rocha et al. 2014).

Some works found in the literature report studies of color removal for the dyes NB and NY in synthetic effluents. Among the methods used are the electro-Fenton process (Fernandes Rêgo et al. 2014) and electrochemical oxidation (Rocha et al. 2012, 2014). Despite presenting satisfactory results, the works employ expensive technologies that demand a long treatment time and, consequently, a higher energy consumption.

Heterogeneous photocatalysis is a process that, through the activation of a semiconductor by sunlight or artificial light, has the ability to decompose polluting organic compounds present in wastewater (Chong et al. 2010). Photocatalysis reactions occur on the surface of photocatalysts (semiconductors) through the pre-adsorption of target compounds on surfaces (Szczepanik 2017). The efficiency of oxidation of organic compounds by radicals will depend on some factors, such as concentration of radicals and contaminant, pH, temperature, type of pollutant, concentration of the semiconductor, dissolved oxygen, presence of ions, type of radiation and light intensity (Chong et al. 2010; Matilainen and Sillanpää 2010). Therefore, it is necessary to carry out studies to optimize operational parameters, providing greater efficiency in the photocatalytic process and, consequently, faster and more economical treatment.

Titanium dioxide (TiO_2) has been one of the most used semiconductors in photocatalysis processes, as it has many advantages, mainly due to the excellent photocatalytic activity. However, its structure on a nanometric scale limits its use due to the occurrence of aggregation of its particles when in suspension, which can decrease its efficiency as a catalyst. With this, TiO_2 has been used after being impregnated in other materials, such as expanded perlite, polymers, zeolites, clay minerals, laminates and glass fibers, activated carbon, among others (Papoulis et al. 2010; Stathatos et al. 2012; Kuang et al. 2019; Silva et al. 2019).

Palygorskite (Pal) is a fibrous clay mineral, a natural inorganic material, abundant in the earth, of low cost and has good adsorption capacity. Several studies found in the literature report the application of palygorskite in environmental remediation processes, in the form of nanostructures, films or membranes, to be used as natural or modified adsorbents and as a support for semiconductors. Previous studies have shown that Pal has a very positive effect on photocatalytic activities, as a support for TiO_2 , and this is due to the ability to avoid possible agglomerations of this semiconductor, as well as contribute to a good adsorptive capacity (Papoulis et al. 2010; Mu and Wang 2016; Al-Mamun et al. 2019; Awad et al. 2019).

The present work has as main objective the application of the Pal- TiO_2 nanocomposite in the environmental remediation of synthetic effluents from NB and NY dyes via heterogeneous photocatalysis. The preparation of the nanocomposite is widely reported in the literature, including its application in the treatment of several types of organic pollutants (Bouna et al. 2011; Chen et al. 2012; Papoulis et al. 2013; Liu et al. 2018; Kuang et al. 2019). However, the synthesis methods reported are time consuming, with the use of different types of reagent, making them expensive. Therefore, the present work also proposes a route for obtaining the simplest Pal- TiO_2 nanocomposite and with fewer steps, using low-cost reagents. Palygorskite was used in its natural form, extracted

in a deposit present in the same region where the dyes are used by textile industries, the northeast region of Brazil. The efficiency of the process in removing color from the dye effluents was evaluated with the application of an experimental design of the central composite design (CCD) type, by estimating the effects of the following operational parameters: UV-C light power, pH of the solution, dye concentration and TiO₂/Pal ratio in the synthesized nanocomposites.

Material and methods

Materials

The palygorskite (Pal) was extracted from a deposit in the Parnaíba basin, in the municipality of Guadalupe (Piauí-Brazil) and was supplied by the company Bentonit União Nordeste. The dyes, Novacron blue C-D (NB) and yellow Novacron C-RG (NY), were supplied by a Brazilian textile industry. The other reagents used were of analytical grade. All aqueous solutions were prepared in distilled water. Table 1 shows some physical and chemical properties of the NB and NY dyes used in this study.

Preparation of the palygorskite-TiO₂ nanocomposite

The titanium impregnation process in the palygorskite was carried out according to Hosseini et al. (2007) (Hosseini et al. 2007) and Silva et al. (2019) (Silva et al. 2019). Palygorskite was used in its natural form and sieved at 100 mesh. The palygorskite and titanium dioxide (TiO₂) were weighed separately, obeying the proportion for synthesis of the two composites Pal-Ti10 and Pal-Ti30, as described in Table 2. TiO₂ was dispersed in ethyl alcohol (99.5%), and then nitric acid (pH 3.5) was added to reduce turbidity and favor dispersion. The mixture was placed in an ultrasound bath for 10 min and then remained under mechanical stirring for 30 min. After filtering, the material was calcined at 450 °C for 30 min. The resulting solid was washed three times with distilled water and dried at 120 °C for 12 h.

Characterization of materials

The characterization of precursor materials (palygorskite and TiO₂) and composites (Pal-Ti10 and Pal-Ti30) obtained in this work had their structures analyzed by Fourier transform infrared spectroscopy (FTIR), X-ray diffraction (XRD), X-ray fluorescence (XRF), scanning electron microscopy (SEM), dynamic light scattering (DLS) and zeta potential (ZP).

Fourier transform infrared spectroscopy (FTIR)

Molecular absorption spectroscopy in the infrared region with Fourier transform (FTIR) contributed to the characterization of the functional groups of chemical compounds. To obtain the infrared spectra, an FTIR-8400S Iaffinity-1 spectrometer was used, in the following specifications: 32 scans; spectrum range 400–4000 cm⁻¹, 4 cm⁻¹ resolution and made in KBr tablets.

X-ray diffraction (XRD)

The X-ray diffraction technique (XRD) was of great importance for the crystallographic identification of the chemical compounds used. To characterize the structure, a Bruker D2Phaser device, CuK α radiation ($\lambda = 1.54\text{\AA}$) with Ni filter, current of 10 mA, voltage of 30kV and Lynxeye detector, was used.

X-ray fluorescence (XRF)

X-ray fluorescence (XRF) analysis was performed on a Bruker S2 Ranger equipment using radiation with Pd or Ag anode, 50 W of power, 50 kV voltage, 2 mA current and XFlash® silicon drift detector.

Scanning electron microscopy (SEM)

The scanning electron microscopy was performed using a Carl Zeiss Auriga model, field emission scanning electron microscope (SEM-FEG). The samples were dried, fixed to the

Table 1 Physicochemical properties of Novacron blue (NB) and Novacron yellow (NY)

Industrial name	Novacron blue C-D	Novacron yellow C-RG
Chemical structure		
Molecular formula	C ₃₄ H ₂₄ N ₆ Na ₄ O ₁₄ S ₄	C ₂₆ H ₁₆ N ₉ Na ₄ O ₁₃ S ₄
Molecular mass	960.794 g/mol	882.664 g/mol
Solubility	Soluble in water	Soluble in water
Absorption in the visible region	600 nm	430 nm
pH (C = 10 mg/L)	6–6.5	5–6

Table 2 Proportion of reagents used to prepare the Pal-Ti30 and Pal-Ti10 composite

Pal-Ti composite	Pal mass (g)	TiO ₂ mass (g)	Ethyl alcohol (mL)	Nitric acid (mL)
10	20	2	150	6
30	20	6	216	18

support using carbon tape and covered with gold forming a thin film over the materials.

Dynamic light scattering (DLS) and zeta potential (PZ).

The determination of the average particle diameter and zeta potential was performed using a Zeta Plus analyzer manufactured by Brookhaven Instruments Corporation. For the analysis, a dispersion of 20 mg was prepared for each sample of Pal, TiO₂ and composites Pal-Ti10 and Pal-Ti30 in 50 mL of ultra-pure water in an ultrasound bath for 20 min. In this analysis, the readings of the dispersed samples were performed in triplicate.

Photocatalytic testing and application of experimental factorial design

For the photocatalysis test, 0.1 g of the composite was weighed and mixed with 200 mL of dye solution. The mixture was taken to the reactor, consisting of a magnetic stirrer and two germicidal lamps, each with a power of 9 W, emitting light in the UV-C range, with a wavelength at 253.7 nm. The total time of the photocatalysis was 4 h, in which aliquots of 3 mL were removed every 30 min to evaluate the time of color removal of the dye, and the aliquot collected was filtered through a CHROMAFIL® 0.20-µm filter for remove the composite dispersed in the sample.

To evaluate the percentage of discoloration, Eq. 1 was used:

$$\text{Color removal (\%)} = [(Abs_0 - Abs_t) / Abs_0] \times 100 \quad (1)$$

where Abs₀ is the initial absorbance and Abs_t is the absorbance at time *t*, obtained on a UV-Vis-NIR spectrophotometer (model Cary 5000 from Agilent Technologies) using quartz cuvettes with 1 cm of optical path, for reading at the wavelength of maximum absorption at 600 nm for NB and 430 nm for NY (visible region).

In the development of the present work, the influence of some operational parameters on the photocatalytic degradation process of the Novacron blue textile dye by the Pal-TiO₂ nanocomposite was evaluated, through the application of experimental design 2⁴ of the central composite design (CCD) type. The parameters evaluated were as follows: titanium dosage in the nanocomposite (10 and 30%), initial

concentration of dye (10 and 30 mg/L), pH of the dye solution (2 and 6) and power of the UV-C lamp (9 and 18 W). The design and validation of the model were obtained with the aid of the software *Protimiza Experimental Design*. Table 3 shows the values used in the CCD for the four factors described previously.

Photocatalytic activity and adsorption tests for NB and YB dyes

The photocatalysis tests under conditions of the optimal parameters were redone, using a time less than 90 min as the maximum photocatalysis time, previously determined with the experimental design of the NB photocatalytic test.

To understand the efficiency of the composite, adsorption tests of the solid were carried out with the dye solution, obeying the best performance conditions: pH 2, 10 mg/L concentration of dye and Pal-Ti30 composite. The test was carried out using 100 mg of composite, 200 mL of dye solution and without UV-C irradiation. The maximum test time was 120 min, in which the adsorption was evaluated at 5, 15, 30, 60, 90 and 120 min.

After determining the adsorption equilibrium time, photocatalysis studies were performed using the optimal conditions and the adsorption time to obtain the photocatalysis kinetic curves for the dyes. For this, they were weighed in a 100-mg beaker of the Pal-Ti30 composite, and 200 mL of dye solution (AZN or AMN) was added. The system was placed in the reactor and previously agitated without using UV-C

Table 3 Values used in the CCD to evaluate four operational parameters in the process of NB photocatalytic degradation by the Pal-TiO₂ nanocomposite

No.	Code	Parameter	Parameter level	
			-1	+1
1	X ₁	Composite (% of TiO ₂)	10	30
2	X ₂	Initial dye concentration (mg/L)	10	30
3	X ₃	pH	2	6
4	X ₄	Potency (W)	9	18

“-1” and “+1” correspond to the lower and upper levels, respectively, associated with each parameter. The response factor (dependent variable) evaluated was “Color removal (%) - Y₁”.

irradiation for 60 min (adsorption equilibrium time); soon after, the lamps were turned on and 3 mL aliquots were removed at 5, 10, 15, 30, 60 and 90 min. Each aliquot was filtered through a CHROMAFIL® 0.20- μm filter and subsequently had their absorbances determined spectrophotometrically.

Photolysis

Photolysis tests were performed for each dye. For this purpose, 200 mL of a 10 mg/L concentration solution of the dyes was prepared and placed in a 250-mL beaker without the presence of the composite, to perform only the study of the effect of UV-C irradiation. Three milliliter aliquots were taken at 5, 10, 15, 30, 60 and 90 min, to compare with the optimal photocatalysis result obtained by experimental design. The aliquots had their absorbance values determined in a molecular absorption spectrophotometer in the UV-vis region, following the maximum absorption length of NB and YB dyes.

Evaluation of the heterogeneous photocatalysis process: kinetic model

Photocatalysis experiments usually follow the Langmuir-Hinshelwood model (Eq. 2) (Stathatos et al. 2012), in which the reaction rate (r) is described as

$$r = -\frac{dC}{dt} = \frac{k_1 KC}{1 + KC} \quad (2)$$

where k_1 is the reaction rate constant, K is the dye adsorption coefficient and C is the dye concentration. When the concentration (C) is very small, the KC factor is negligible, and the equation can be rewritten describing a pseudo-first order kinetics.

The apparent velocity constant (K_{app}) for the photocatalysis process for each dye was estimated according to the result obtained with the application of the pseudo-first order kinetic equation (Eq. 3) (Silva et al. 2019; Tomul et al. 2019).

$$\ln\left(\frac{C_0}{C}\right) = K_{\text{app}} \cdot t \quad (3)$$

where, C_0 and C are the concentrations of dyes in the initial time and time t (when the photocatalysis ended), respectively. The K_{app} value can be determined using the graph line equation that relates time (t) versus $\ln(C_0/C)$, corresponding to the slope of the line.

Total organic carbon (TOC)

Samples collected after the end of the photocatalysis process had their percentages of total organic carbon (TOC) determined in an Analytic Jena Multi N/C 3100 equipment. The equipment can measure the amount of total carbon

(TC) and inorganic carbon (IC). TOC is given by subtracting TC and IC.

Analysis of degradation by-products by gas chromatography coupled to mass spectrometry (GC-MS)

The by-products of the photocatalytic degradation of both dyes were identified by gas chromatography analysis (model Shimadzu—GC-2010 Plus) coupled to a mass spectrometer (QP2020). Samples for GC-MS analysis were prepared from an extraction using 4 mL of solvent (1:1 mixture—hexane and dichloromethane) and 1 mL of the product of each dye after photocatalytic activity. The sample was filtered over anhydrous sodium sulfate and subsequently also filtered through a syringe with a Teflon membrane (PTFE) with hydrophobic treatment (diameter of 25 mm and pore of 0.22 μm), to eliminate traces of water. Samples were injected into the chromatograph.

The conditions used in the GC-MS analysis are described in Table 4.

Results and discussion

Characterization of Pal-TiO₂ nanocomposites

FTIR

The molecular absorption spectra in the infrared region for Pal, TiO₂, Pal-Ti10 and Pal-Ti30 are shown in Figure 1.

From the analysis of the spectrum referring to the Pal, it was possible to observe three bands in 3622 cm^{-1} , 3581 cm^{-1} and 3547 cm^{-1} , which are associated with the vibrational stretching of groups O–H in bonds with octahedral cations (Al, Mg or Fe)–OH. The widened band between 3499 and

Table 4 Conditions used in the GC-MS analysis

Column	SH-Rtx-5MS (30 m \times 0.25 mm \times 0.25 μm)
Composition	5% dimethyl/95% polysiloxane
Heating ramp	40 $^{\circ}\text{C}$ (5 min) 7 $^{\circ}\text{C}/\text{min}$ to 180 $^{\circ}\text{C}$ (5 min) 5 $^{\circ}\text{C}/\text{min}$ to 280 $^{\circ}\text{C}$ (5 min)
Injector temperature	230 $^{\circ}\text{C}$
Carriers gas	Helium
Gas flow	1 mL/min
Injection mode	Splitless
Ion source temperature	230 $^{\circ}\text{C}$
Transfer line temperature	250 $^{\circ}\text{C}$
Mass range	50 to 500 m/z

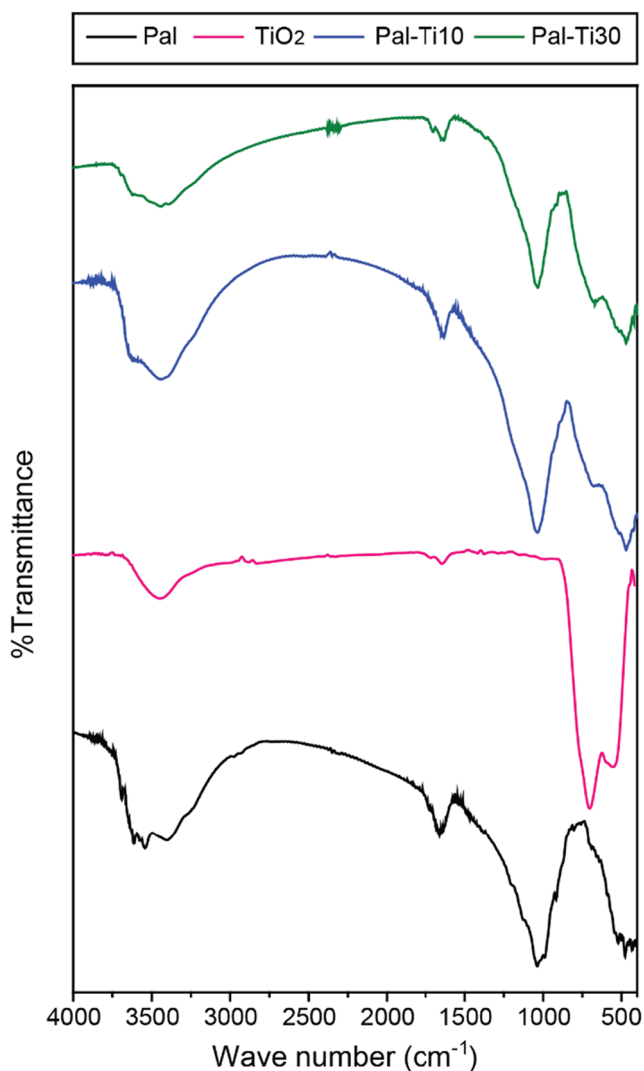


Fig. 1 Infrared absorption spectra for Pal, TiO₂, Pal-Ti10 and Pal-Ti30

3361 cm⁻¹ was attributed to the vibrations of OH groups of water molecules, and in 1651 cm⁻¹ it was attributed to the angular deformations of OH of the water adsorbed on the surface and in the zeolitic channels present in the palygorskite. The bands at 987 cm⁻¹ and 1033 cm⁻¹ were attributed to the vibrational deformation of the O–Si–O bond. The other bands at 791 cm⁻¹ and 910 cm⁻¹ refer to the folding of OH bonds in octahedral cations (Chang et al. 2009; Xavier et al. 2012; Shi et al. 2017; Damasceno Junior et al. 2020c, b).

The absorption spectrum obtained for TiO₂ showed a wide band with low intensity at 3441 cm⁻¹, attributed to the OH groups that are present in TiO₂, as well as the presence of water molecules that can also be attributed to the appearance of a band in 1630 cm⁻¹ (Nguyen and Juang 2019). It is also possible to observe two intense bands at 539 and 686 cm⁻¹, referring to the deformations of the O–Ti–O bonds, which characterize the crystalline phase anatase titanium (Silva et al. 2019).

Observing the spectra referring to the composites Pal-Ti10 and Pal-Ti30, it is possible to notice the occurrence of the intensity decrease in the bands between 3700 and 3400 cm⁻¹, disappearing some bands that corresponded to the stretches of the OH group on the surface of the palygorskite. From the increase in TiO₂ in the composite synthesis process, it is noticed that the intensity of the broadband in 3700 to 3400 cm⁻¹ decreased. It is proposed that titanium may be replacing water molecules and OH groups in the palygorskite. The decrease in intensity by 1651 cm⁻¹ was also observed, and by increasing the amount of titanium in the composite, the band gradually lost its intensity, and it can be concluded that the titanium possibly occupied a certain space in the palygorskite channels. The band corresponding to the stretching of the Si–O bond by 1033 cm⁻¹ prevailed in the other spectra and only suffered a decrease in its intensity due to the impregnation of titanium; however, other bands such as 791, 910 and 987 cm⁻¹ were not detected in the spectra of the composites, perhaps caused by the presence of TiO₂. A new band appeared at 679 cm⁻¹ for the Pal-Ti10 and 664 cm⁻¹ for the Pal-Ti30, characteristic of the deformations in the O–Ti–O connections, as well as the band at 462 cm⁻¹ for both composites, more defined and which is also related to the O–Ti–O bonds of the crystalline structure of TiO₂ (Papoulis et al. 2010; Zhang et al. 2019).

XRD and XRF

Figure 2 shows the diffractograms obtained in the XRD analysis for Pal, TiO₂, Pal-Ti10 and Pal-Ti30.

The diffractogram obtained for Pal showed well-defined reflections, as it is a crystalline material. The first peak, at 2θ equal to 8.5°, corresponds to the basal spacing (interplanar distance) of the palygorskite, which provides the value of 1.029 nm and corresponds to the plane (110). The remaining peaks at 12.6°, 19.9°, 27.7° and 34.6° (2θ) correspond to the crystalline planes of Si–O–Si, (200), (121), (400) and (161), respectively. Reflections corresponding to the presence of quartz as an impurity at 21.1° and 26.8° were also identified, which was expected, since the mineral clay was used without any pretreatment (Xavier et al. 2012; Shi et al. 2017; Xu et al. 2017; Damasceno Junior et al. 2020c, b).

The reflections for TiO₂ were characteristic of the crystallinity of its tetragonal anatase structure, in which peaks were observed in 2θ equal to 25.5°, 37°, 48.0°, 59.9° and 54.8°, with their respective planes (101), (004), (200), (105) and (214). The basal spacing for the plane (101) was 0.35 nm. TiO₂ has three types of structure (polymorph): anatase, rutile and brookite, with anatase being the form that presents better photocatalytic activity and greater thermodynamic stability (Baccaro et al. 2019; Silva et al. 2019; Zhang et al. 2019; Nguyen et al. 2020).

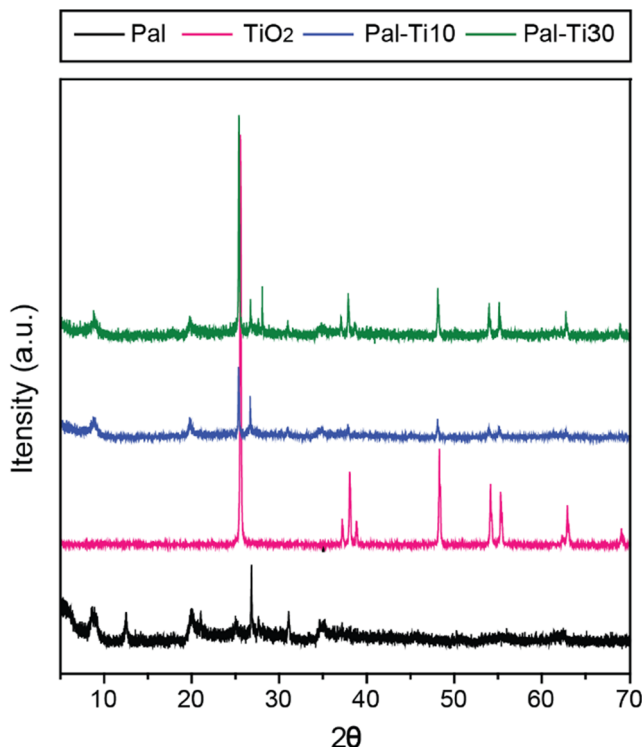


Fig. 2 X-ray diffractograms for Pal, TiO₂, Pal-Ti10 and Pal-Ti30

Comparing the diffractograms of Pal and TiO₂ with those of the composites Pal-Ti10 and Pal-Ti30, it is observed that the characteristic peaks of pure materials were detected. The characteristic reflections of Pal and the main reflections characteristic of TiO₂ were observed. This shows that the composites formed had TiO₂ deposited on the structure of Pal, since it is possible to identify very clearly reflections characteristic of its anatase form. As well, it is observed that the intensity of the characteristic peaks of TiO₂ has its intensities increased as the amount of TiO₂ incorporated in the synthesis increases.

The semi-quantitative chemical composition determined by X-ray fluorescence (XRF) for PAL, Pal-Ti10 and Pal-Ti30 is shown in Table 5.

Pal presented in its composition a higher percentage of Si, which characterizes the silicates present in the tetrahedron leaves of clay minerals and quartz, corroborating the results obtained in the DRX. Others that appeared in greater quantity were Fe and Al, in which the palygorskite is formed mainly by sheets of octahedron coordinated by aluminum cations, with greater isomorphous substitutions by iron cations. This is due to the fact that the soil is rich in iron in the deposit where the palygorskite was extracted (Xavier et al. 2012; Dos Santos et al. 2013).

The composites Pal-Ti10 and Pal-Ti30 presented a higher content of titanium (Ti), confirming the data obtained previously by DRX. It was observed that as the amount of Ti increased in the composite synthesis, there was a greater incorporation of semiconductor in Pal. In addition to the

Table 5 Chemical composition of Pal clay and nanocomposites Pal-Ti10 and Pal-Ti30

Element	Pal	Pal-Ti10	Pal-Ti30
	Content (%)		
Si	38.10	30.73	20.54
Al	21.27	18.13	12.69
Fe	25.71	22.30	19.11
K	7.08	5.68	4.09
Mg	2.99	2.35	1.69
Ca	2.47	2.21	1.36
Ti	1.47	17.63	39.66
Others*	< 1%		

*Mn, V, Zr, Zn and Sr

deposition of TiO₂ on Pal, the significant drop in the percentage of oxides of Si (IV), Al (III) and Fe (III or II) may have happened due to possible isomorphous substitutions of these cations for Ti⁴⁺ cations. This process is facilitated when cations have similar size, charge and properties (Moraes et al. 2017).

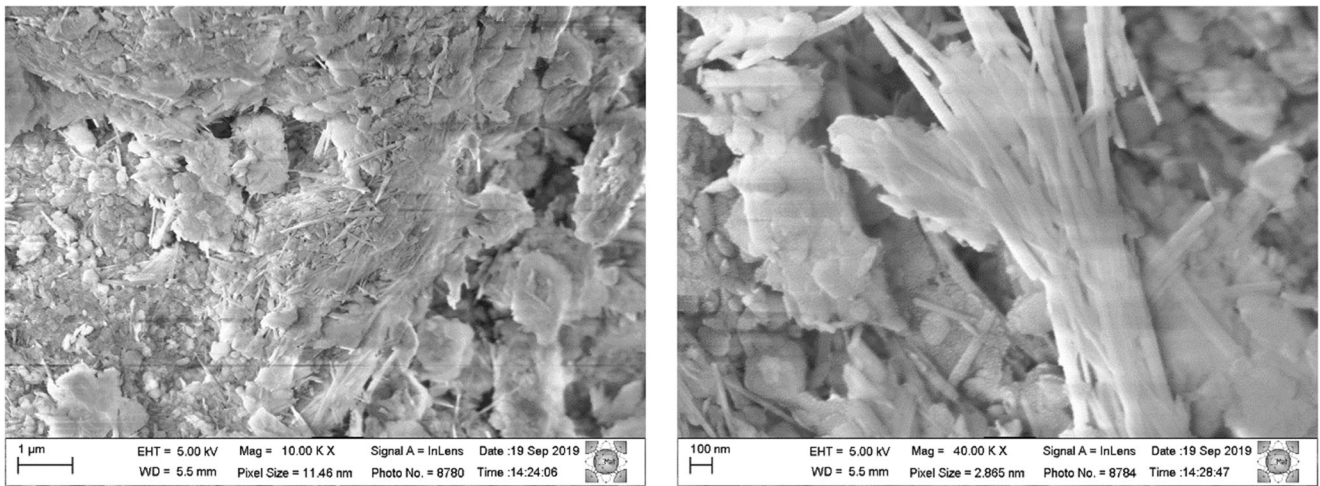
SEM

Figure 3 shows the micrographs for the PAL sample (Figure 3a), TiO₂ (Figure 3b) and the composites Pal-Ti10 and Pal-Ti30 (Figure 3c,d). The morphologies of the materials (precursors and composites) were characterized by scanning electron microscopy. In Figure 3a, it is possible to observe that PAL presents its typical fibrous morphology, presenting its fibers aggregated in some regions, entangled in planar structures. This morphology has also been identified in other works in the literature (Papoulis et al. 2010; Dos Santos et al. 2013; Damasceno Junior et al. 2020b). The fibers were needle-like and varied in length, less than 1 μm. In Figure 3b, it was observed that the fine powder of TiO₂ presented a morphology compared to agglomerated spheres.

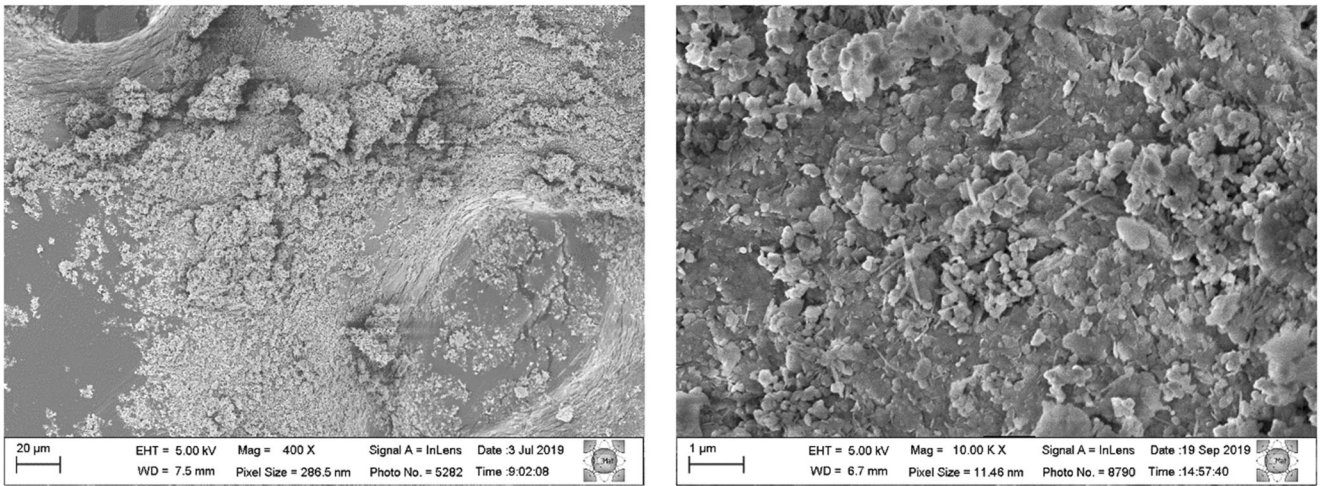
In the micrographs of the composites Pal-Ti10 and Pal-Ti30 (Figure 3c, d), the TiO₂ particles are deposited on the surface of the palygorskite. In Figure 3c, the Pal-Ti10 composite shows little TiO₂ distributed along the fibers; however, in Figure 3d, it is observed that the Pal-Ti30 composite shows in the micrograph that TiO₂ is noticeably in greater quantity on the fibers of the palygorskite.

Zeta potential and particle size

The zeta potential data for the study materials at pH equal to 7 can be seen in Table 6. The values obtained resulted in negative potentials, which shows materials having surfaces with negative charges, in accordance with the literature (Silva et al.

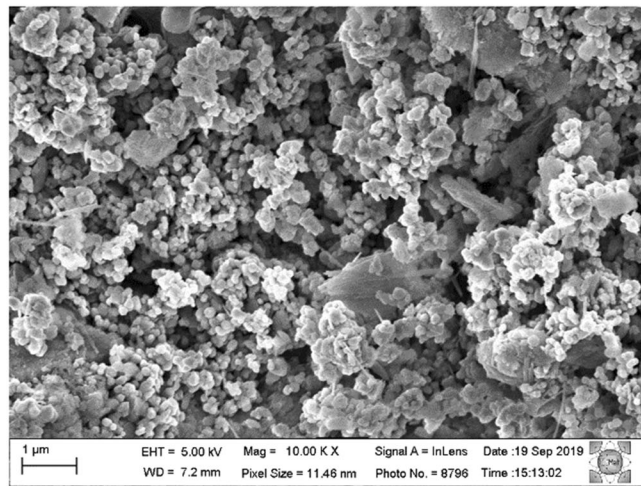


(a)



(b)

(c)



(d)

Fig. 3 Micrographs for Pal (a), TiO₂ (b) and the composites Pal-Ti10 (c) and Pal-Ti30 (d)

Table 6 Zeta potential values obtained (mean \pm standard deviation) for the palygorskite (Pal), TiO₂ and for composites (Pal-Ti10 and Pal-Ti30)

Material	Zeta potential
Pal	-23.79 ± 0.77
TiO ₂	-13.84 ± 1.53
Pal-Ti10	-24.04 ± 0.89
Pal-Ti30	-36.53 ± 1.36

2019; Damasceno Junior et al. 2020a, b). According to Gouvêa and Murad (2001) (Gouvêa and Murad 2001), the larger the zeta potential modulus of a material, the more stable the particles will be, that is, there will be less probability of flocculation or agglomeration.

Analyzing the synthesized composites and comparing them to pure palygorskite and TiO₂ materials, which presented zeta potential equal to -23.79 mV and -13.84 mV, respectively, it was possible to notice that the zeta potential value for Pal-Ti10 (-24.04 mV) remained close to the palygorskite's zeta potential value. Thus, it can be said that the incorporation of TiO₂ in palygorskite was a good strategy, since it made the dispersion of the titanium particles more stable in aqueous solution. The increase in modulus was significantly greater for the Pal-Ti30 composite, as it corresponded to a potential of -36.53 mV. This result was of great importance, as it shows that the increase in the amount of titanium dioxide results in a more stable composite, and it is possible to predict better performance in the photocatalysis process.

Table 7 shows the values obtained by the gaussian distribution for the average particle size of the materials in the present study under ambient conditions of temperature and pressure, obtained by dynamic light scattering (DLS).

The average values for the particle size of all materials were presented in nanometric order and are consistent with values recorded in the literature. The particle size of the palygorskite showed results consistent with those described in the literature, since it presented values below $1 \mu\text{m}$ (Papoulis et al. 2010). Compared to the results obtained by Dos Santos Soares et al. (2013), the palygorskite presented in this study had a particle size in the same order of magnitude (approximately 500 nm), but with a smaller value, that is, it had a smaller particle diameter, which was a favorable result, indicating a material with a larger contact surface..

Table 7 Particle size values (mean \pm standard deviation) for palygorskite (Pal), TiO₂ and composites (Pal-Ti10 and Pal-Ti30)

Material	Particle size (nm)
Pal	340.7 ± 14.0
TiO ₂	63.7 ± 4.9
Pal-Ti10	364.0 ± 10.6
Pal-Ti30	307.9 ± 7.8

The synthesized composites had their values close to the average particle size of the natural palygorskite. Comparing the two composites, it was observed that there was a decrease in the particle size value for the Pal-Ti30 composite. This has also been observed by other works in the literature to support the titanium dioxide composite in other materials (Silva et al. 2019).

Photocatalytic activity

Experimental design for evaluating the color removal of the NB dye

The photocatalytic activity of the Pal-Ti10 and Pal-Ti30 composites was evaluated by decolorizing the NB dye under ultraviolet irradiation (UV-C), and a factorial experimental design was followed to determine parameters that interfere in the photocatalysis process. Subsequently, the parameters that conditioned better performance in the photocatalytic activity were applied to the NY dye.

The literature reports the existence of several factors that interfere in the photocatalytic process, among them: the method of synthesis, the quantity, crystalline form and contact surface of the catalyst; the pH of the solution, the concentration of the pollutant, temperature, oxygenation, intensity of UV irradiation, among others (Matilainen and Sillanpää 2010; Bamba et al. 2017).

Table 8 presents the planning matrix, with the response values obtained in each experiment.

Table 9 shows the values for the coefficients, the standard error, the Student distribution point (t) and the p values (level of significance) obtained for the variables studied using the linear regression technique. Considering a 95% confidence level and, consequently, a 5% significance level, we have that, for the main effect of a variable or the interaction effect to be considered significant, the p value must be less than 0.05 (Barros Neto et al. 2010; Rodrigues and Iemma 2014). Therefore, as noted in the table, the effects for all variables and the interaction effect $X_1 \cdot X_3$, can be considered significant.

The relationship between the answer (dependent variable) and the four main parameters can be described by a first-order empirical polynomial equation (Barros Neto et al. 2010; Rodrigues and Iemma 2014). Thus, Eq. 4 describes the color removal predicted by the model as a function of the variables that showed statistical significance. The model was built from coded values.

$$Y_1 = 67.83 + 4.77X_1 - 19.66X_2 - 13.37X_3 + 6.62X_4 + 2.31X_1X_3 \quad (4)$$

Figure 4 shows the graph of adjustment of the theoretical model to the data obtained experimentally. We can observe a certain normality, in which there are no points very distant

Table 8 Color removal results (Y_1) for the NB dye obtained with the application of the experimental design

Experiment	Composite (X_1 , % of TiO_2)	Initial dye concentration (X_2 , mg/L)	pH (X_3)	Potency (X_4 , W)	Color removal* (Y_1 , %)
1	30	30	2	9	55.0 ± 11.3
2	10	10	2	18	100.0 ± 0.0
3	10	30	2	9	48.1 ± 15.3
4	30	10	6	18	100.0 ± 0.0
5	30	10	2	18	100.0 ± 0.0
6	30	10	2	9	100.0 ± 0.0
7	30	30	2	18	79.6 ± 6.2
8	10	30	2	18	66.8 ± 5.0
9	10	30	6	18	32.6 ± 0.7
10	10	10	6	9	56.9 ± 4.3
11	30	30	6	18	43.6 ± 1.7
12	30	30	6	9	32.5 ± 3.7
13	10	10	6	18	72.9 ± 3.1
14	30	10	6	9	70.1 ± 2.7
15	10	10	2	9	100.0 ± 0.0
16	10	30	6	9	27.0 ± 0.9

*Mean ± standard deviation

from the line. Thus, it can be inferred that there is a good agreement between the experimental results and the results predicted by the model (Barros Neto et al. 2010; Rodrigues and Iemma 2014).

The significance attested previously by the values presented in Table 9 can be confirmed by analyzing the Pareto graph (Figure 5). The horizontal line represents the t value (Student distribution point) tabulated, and the vertical bars calculated t values, associated with each variable, at a 95% confidence level. Therefore, as observed in the graph, we can attest that all the main effects and the interaction effect $X_1 \cdot X_3$ can be

Table 9 Estimated regression coefficients and corresponding t and p values obtained during the central composite design for the photocatalytic degradation of NB by the TiO_2 /palygorskite nanocomposite

Name	Coefficient	Standard error	t calculated	p value
Mean	67.83	1.16	58.70	0.0000
X_1	4.77	1.16	4.13	0.0002
X_2	-19.66	1.16	-17.01	0.0000
X_3	-13.37	1.16	-11.57	0.0000
X_4	6.62	1.16	5.73	0.0000
$X_1 \cdot X_2$	-0.26	1.16	-0.23	0.8213
$X_1 \cdot X_3$	2.31	1.16	2.00	0.0527
$X_1 \cdot X_4$	1.58	1.16	1.36	0.1810
$X_2 \cdot X_3$	-0.86	1.16	-0.74	0.4625
$X_2 \cdot X_4$	0.88	1.16	0.76	0.4514
$X_3 \cdot X_4$	1.20	1.16	1.04	0.3043

considered significant, since the bars are above the tabulated t value (Barros Neto et al. 2010; Rodrigues and Iemma 2014).

Table 10 presents the values for the analysis of variance of the model obtained in the present work.

Analyzing the table previously presented for the Y_1 answer, we found that the regression was highly significant ($p < 0.0000$). For the model to be considered statistically valid, the F calculated for the regression must be greater than the tabulated F value. The F obtained for the lack of adjustment must be less than the value of table F (Barros Neto et al. 2010; Rodrigues and Iemma 2014; Hassani et al. 2015).

The F value for the regression, according to the degrees of freedom for the regression and for the residuals, is 2.45 (5% significance level). Thus, we can attest that the model is statistically valid, since the F calculated for the regression has a

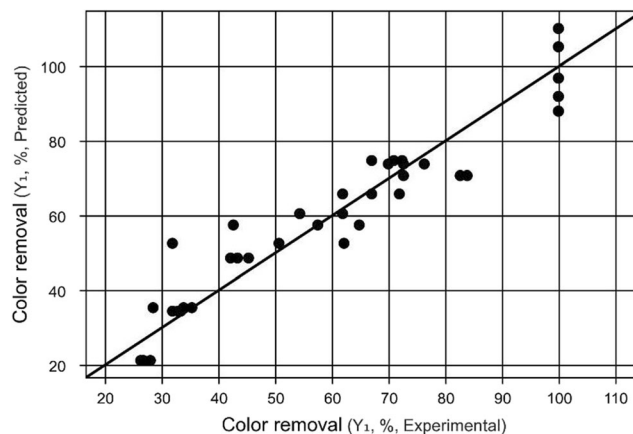


Fig. 4 Graph of experimental values versus predicted values

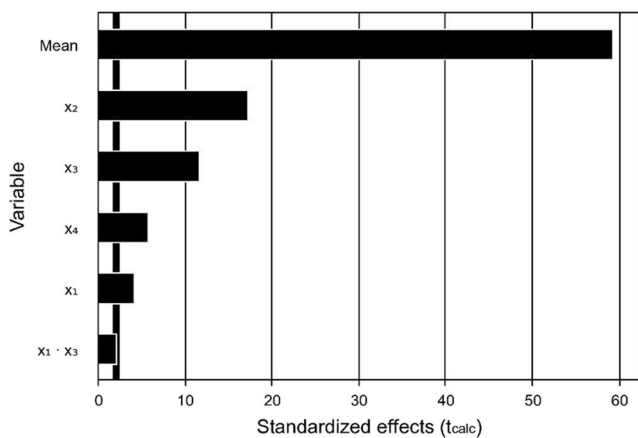


Fig. 5 Pareto graph

considerably higher value. In relation to the *F* table for the lack of adjustment, according to the degrees of freedom for the lack of adjustment and for the pure error, it is 2.16 (5% significance level). The calculated *F* value was higher than the tabulated one, confirming the model’s proven validity (Barros Neto et al. 2010; Rodrigues and Iemma 2014).

The regression model also showed a high determination coefficient ($R^2 = 92.06\%$), which implies that 92.06% of the variations in dye removal can be explained by the model. Only 7.94% of the variations cannot be explained. This quite satisfactory value also attests to the statistical validity of the model obtained. Therefore, we can obtain the response surfaces for our model, which will be presented below (Barros Neto et al. 2010; Rodrigues and Iemma 2014; Hassani et al. 2015).

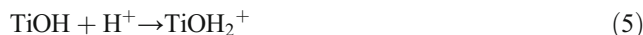
The response surfaces obtained from the model are shown in Figure 6.

From the analysis of the response surface (Figure 6) and the coefficient values presented in Table 9, we can report the following observations: (i) The variables X_1 and X_4 (titanium concentration in the composite and power, respectively) had a positive effect, indicating that by increasing the titanium concentration in the composite and the incidence of UV-C radiation, the color removal (%) is maximized; (ii) The variables X_2 and X_3 (pH and concentration, respectively) showed negative values. Thus, we can infer that greater responses (color removal) are obtained when the values of both variables are minimal.

Therefore, the operational variables chosen for the photocatalytic degradation process of NB and NY dyes, optimized from the experimental design were Pal-Ti30 composite, pH 2, 18 W of UV irradiation and 10 mg/L concentration.

When using the composite containing 30% TiO_2 , better results were obtained in the photocatalytic process, as was also observed in a work previously published by the group (Silva et al. 2019). According to reports presented by Bamba et al. (2017) (Bamba et al. 2017), there is a mass considered optimum of the photocatalyst to be used, and that allows an improvement in the capitation of ultraviolet irradiation. The amount of semiconductor used can influence the rate of degradation of the pollutant and, if values are placed more than ideal, it can cause a negative effect on photocatalytic activity, since high concentrations of TiO_2 can generate high turbidity and, thus, make it difficult the penetration of UV irradiation in the solution (Matilainen and Sillanpää 2010).

As seen in the results of the experimental design, acidification of the solution to reach pH 2 improved the photocatalytic process applied to the NB dye, classified as reactive and that has the azo group in its chemical structure. The pH of the solution in this effluent treatment method is of great importance because it affects the surface charge of TiO_2 , as well as influences the aggregation of TiO_2 nanoparticles. Depending on the type of pollutant, the pH variation can have a positive or negative impact on the color removal result. Equations 5 and 6 show the influence of the solution’s pH on the surface charge of TiO_2 . When TiO_2 is in acidic conditions, its surface is positively charged and, in alkaline conditions, it will have a negatively charged surface (Bamba et al. 2017).



However, not only TiO_2 will be influenced by the pH of the medium, but also the pollutant treated in the process, providing ionization of its structures. For pollutants considered anionic, as is the case of the dyes studied in this work, the rate of degradation will tend to increase in acidic solutions and decrease in alkaline solutions (Bamba et al. 2017).

The concentration of the pollutant influences the photocatalytic activity, since the color removal or percentage degradation

Table 10 ANOVA for the answer (Y_1)

Variation source	Sum of squares	Degrees of freedom	Mean square	F value	p value
Regression	30,579.4	5	6115.9	97.5	0.00000
Residuals	2635.8	42	62.8	-	-
Lack of fit	1681.6	10	168.2	5.6	0.00008
Pure error	954.2	32	29.8	-	-
Total	33,215.2	47	-	-	-

$R^2 = 92.06\%$

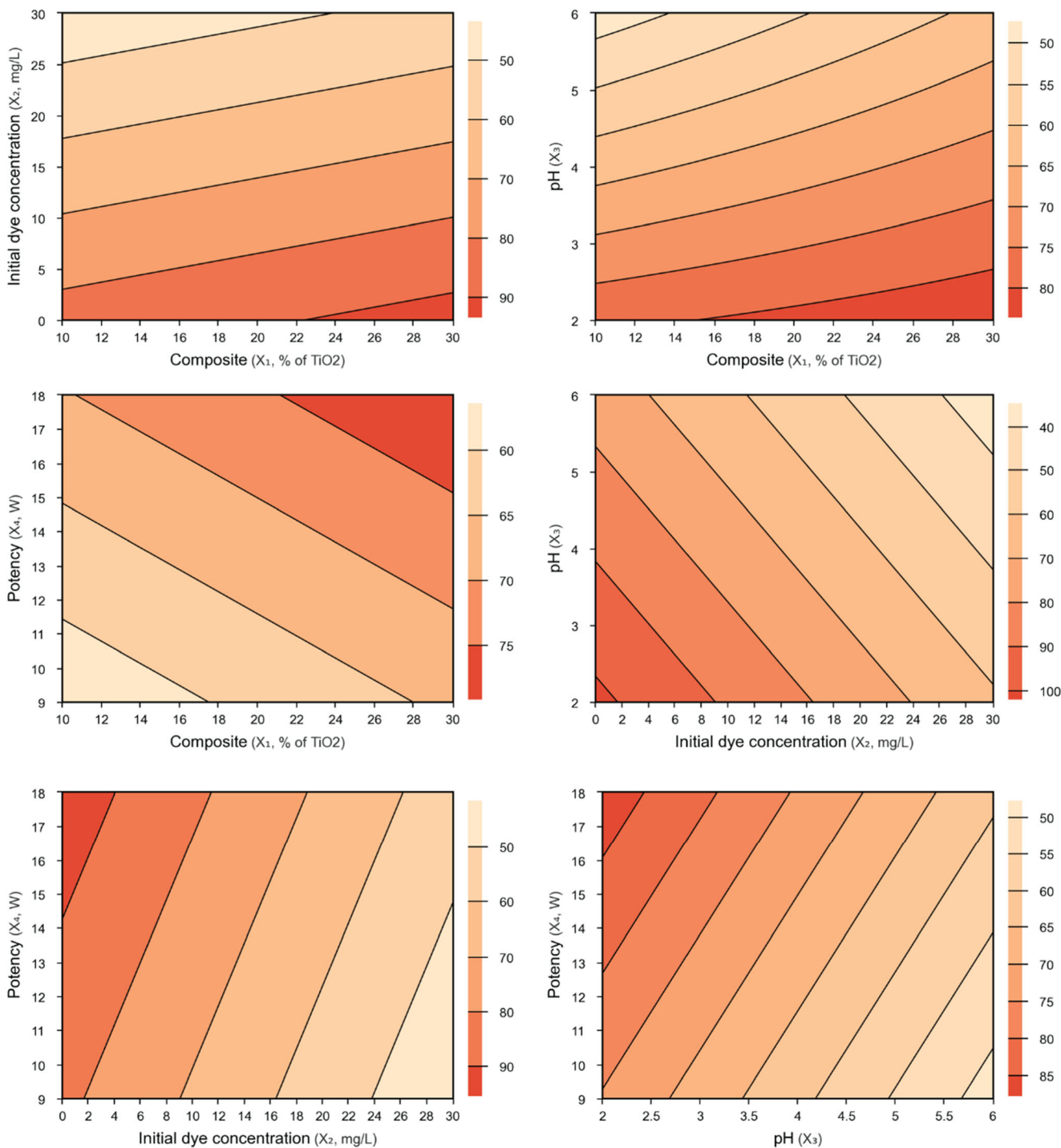


Fig. 6 Response surfaces for color removal (%) of the NB dye as a function of the experimental parameters studied

decreases with the increase in the concentration of the pollutant. The effects that decrease the photocatalytic activity can be varied; one of these effects is caused by the adsorption of the dye in the solid that can provide little contact surface of the catalyst to capture UV radiation. In addition, there is a decrease in the formation of oxidizing radicals, as the active sites may be occupied by pollutant molecules. Another effect is that the large amount of pollutant decreases the penetration of ultraviolet light (Reza et al. 2017).

In studies carried out with other reactive dyes, it was observed that the increase in radiation intensity, using TiO_2 as a catalyst, provided an increase in the percentage of degradation, which was also observed in this work, in which a better response was obtained at a higher intensity radiation. This is due to the fact that at high light intensities the electron gap formation is predominant and the recombination is insignificant (Reza et al. 2017).

Photocatalysis and photolysis tests under optimized conditions

The photolysis tests were performed using the conditions of dye solutions with concentration 10 mg/L, pH 2 and power of 18 W. The photolysis results were important for investigating the degradation provided only with the use of the UV-C irradiation lamp. The analysis by photocatalysis was performed using, in addition to the parameters mentioned in the photolysis, the Pal-Ti30 composite.

The results of photocatalysis of the dyes showed excellent results of color removal. In Figure 7, it is possible to observe the color of the solution before and after the photocatalysis process for the dyes NB (Figure 7a) and NY (Figure 7b). It is noted that after the photocatalysis test the synthetic effluent was clear. The same can be observed from the analysis of the molecular absorption spectra in the visible region for both dyes (Figure 9), evidenced by the disappearance of the absorption band in the wavelength for each dye over the test time.

When comparing the photodegradation process with and without the use of catalyst, it becomes evident that the time is significantly reduced to obtain the absorbance decays corresponding to the dyes' chromophores, as seen in Figure 8.

Photocatalysis showed a higher efficiency of dye degradation over time, since the presence of the catalyst accelerated the formation of oxidizing radicals in the photodegradation systems. The photolysis process for dyes requires a long reaction time; thus, it becomes unfeasible to remove the color of dyes, since in 90 min a color removal corresponding to only 30% of the initial color was obtained. On the other hand, the

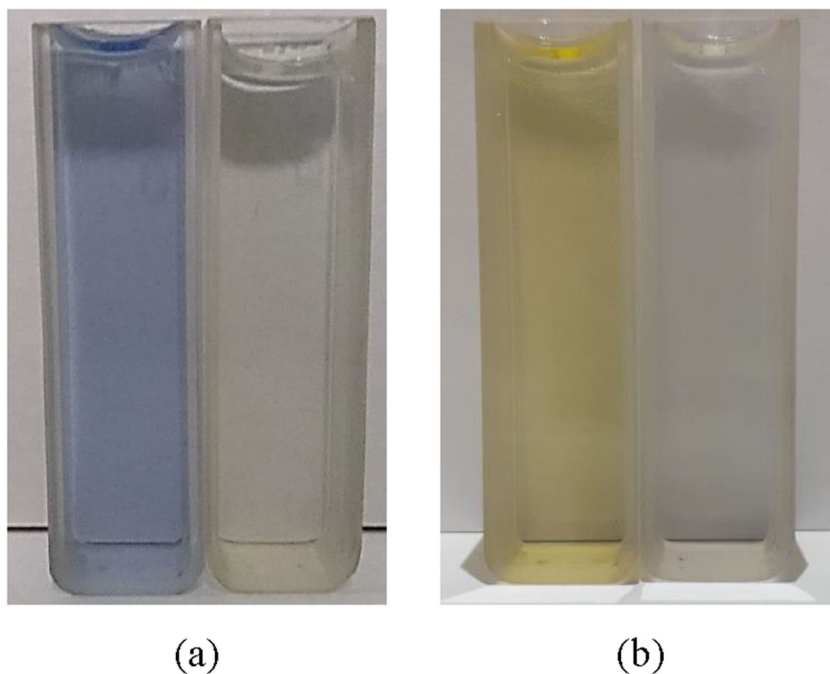
results of photodegradation using the Pal-Ti30 catalyst, in a time of 90 min, obtained 100% discoloration.

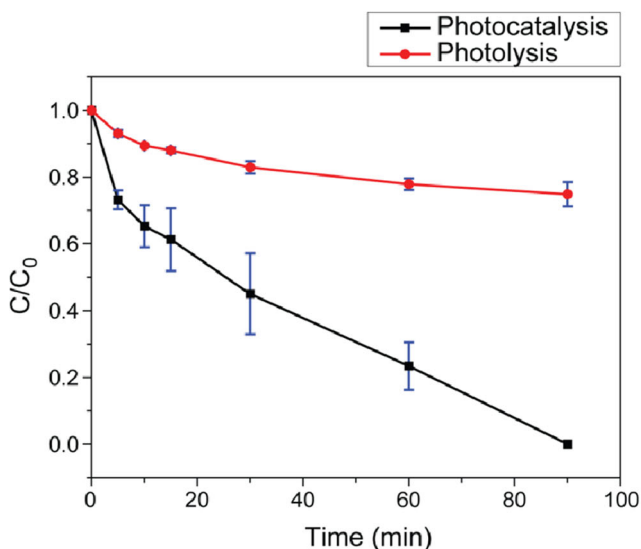
Silva et al. (2019) (Silva et al. 2019) investigated the color removal by photocatalysis of the remazol red dye, which is also an azo dye, using an expanded perlite/titanium dioxide composite, and its color removal values reached 100% in about 210 min. Rocha et al. (2014) (Rocha et al. 2014), using the electrochemical method with Pt/Ti anode, managed to remove 100% of Novacron yellow dye in 480 min.

In the present study, for both dyes, the results of the photocatalysis were quite similar, showing that the use of TiO₂ can be quite efficient in the photodegradation of chromophores in industrial dyes of the azo type. The first decay for NB and NY dyes (Figure 8) is a more intense, since the composite is formed by porous materials and has a good adsorption capacity. Reactive dyes may have a certain affinity for clay minerals such as palygorskite, as they have hydroxyl groups on their surface that can interact with the amino groups contained in the dyes through hydrogen bonding interactions and Van der waals forces (Hassan and Carr 2018; Damasceno Junior et al. 2020b). Thus, before the start of photocatalysis, the adsorption of part of the dye occurs in a previously determined time of approximately 60 min.

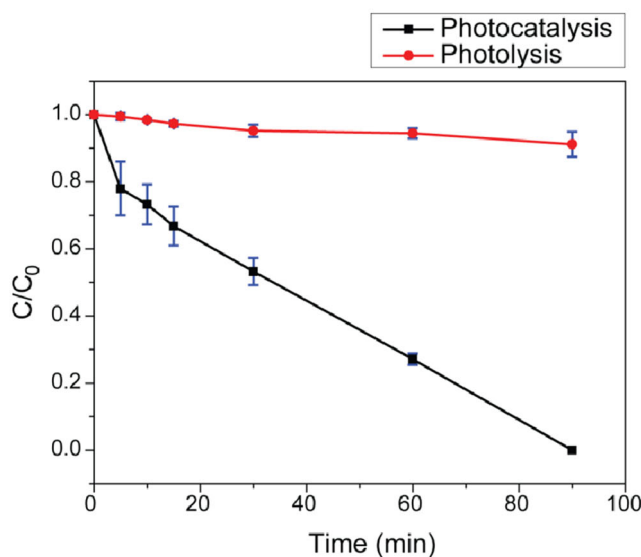
Comparing the spectra illustrated in Figures 9 and 10, in 90 min, for the NB dye, there was a 100% and 26% color removal, by photocatalysis (Figure 9a) and by photolysis (Figure 10a), respectively. While for NY dye, it was 100% and 5%, by photocatalysis (Figure 9b) and by photolysis (Figure 10b), respectively. Therefore, the presence of the catalyst is an extremely important factor for the efficiency of

Fig. 7 Visual aspect of the solution of dye NB (a) and dye NY (b) before and after the photocatalysis process





(a)



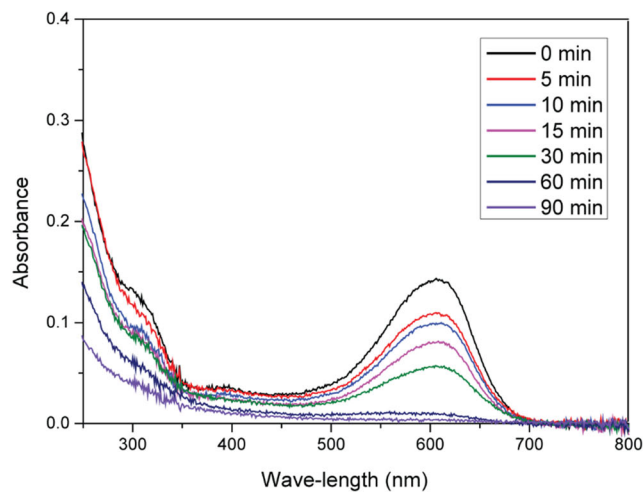
(b)

Fig. 8 Color removal efficiency versus photoreaction time for NB (a) and NY (b)

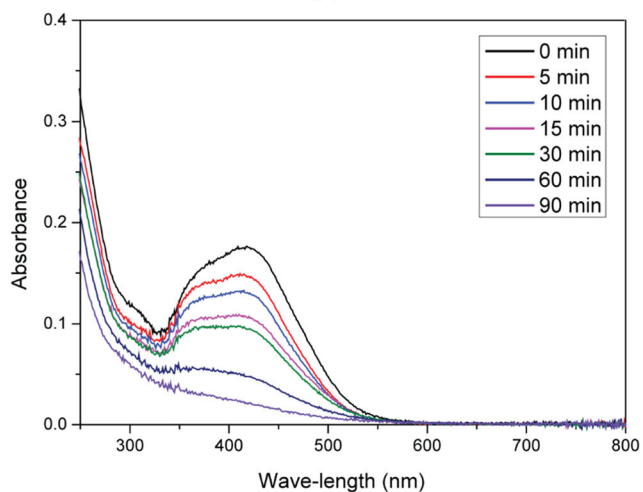
photodegradation, since it increases the rate of formation of oxidative radicals and, consequently, the efficiency in the process of removing color from effluents (Matilainen and Sillanpää 2010).

Kinetic study

Most organic compounds follow the pseudo-first order kinetics that starts from the Langmuir-Hinshelwood equation, so it was applied to the results of both dyes. This model is suitable for the analysis of photoreactions with low concentrations of contaminants; thus, we have a model that depends directly on the concentration of



(a)



(b)

Fig. 9 Molecular absorption spectra in the visible region along the photocatalytic process for NB (a) and NY (b) dyes, experimental conditions: Pal-Ti30 composite, pH 2, 18 W potency and 10 mg/L dye concentration

the degraded substance (Silva et al. 2019). The graphs were plotted relating $\ln(C_0/C)$ and time (min) in order to determine the values of the apparent velocity constants (K_{app}) given in min^{-1} .

Figure 11 shows the plots of the kinetic model for the photocatalysis and photolysis process of NB (Figure 11a) and NY (Figure 11b) dyes. Analyzing the curves, it was observed that the lines for photocatalysis of both dyes presented a slope (slope) greater than that of photolysis. The values of the slope correspond to the values of the K_{app} , and this implies that the increase in the constant shows that the degradation using the presence of catalyst improves the photodegradation activity. The results become more evident when analyzing the decolorization efficiency, that it was possible to obtain a 100% color removal for the dyes.

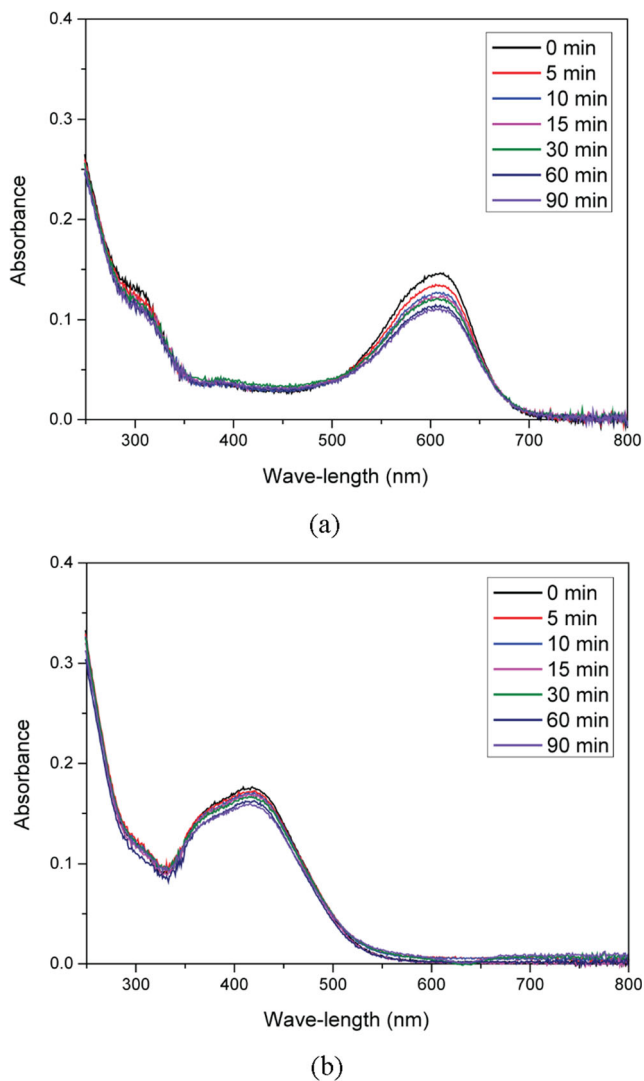


Fig. 10 Molecular absorption spectra in the visible region along the photolysis process for NB (a) and NY (b) dyes, experimental conditions: Pal-Ti30 composite, pH 2, 18 W potency and 10 mg/L dye concentration

The correlation (R^2) and K_{app} values are listed in Table 11 for photolysis and photocatalysis. The correlation values adequately fit the linear equation of the kinetic method used, and the results obtained by photocatalysis showed a better fit to the model than photolysis. Already the values of the constant K_{app} increased singularly in the photocatalysis when compared to the photolysis, result of the efficiency of color removal provided by the composite Pal-Ti30. The K_{app} constant is very important in the kinetic study, since it indicates how favorable the degradation product formation is in the photocatalysis reaction. Therefore, the increase in the constant from the photocatalysis results indicates that the process becomes more efficient with the use of the catalyst and the lamp than with the use of only the UV-C lamp (Silva et al. 2019).

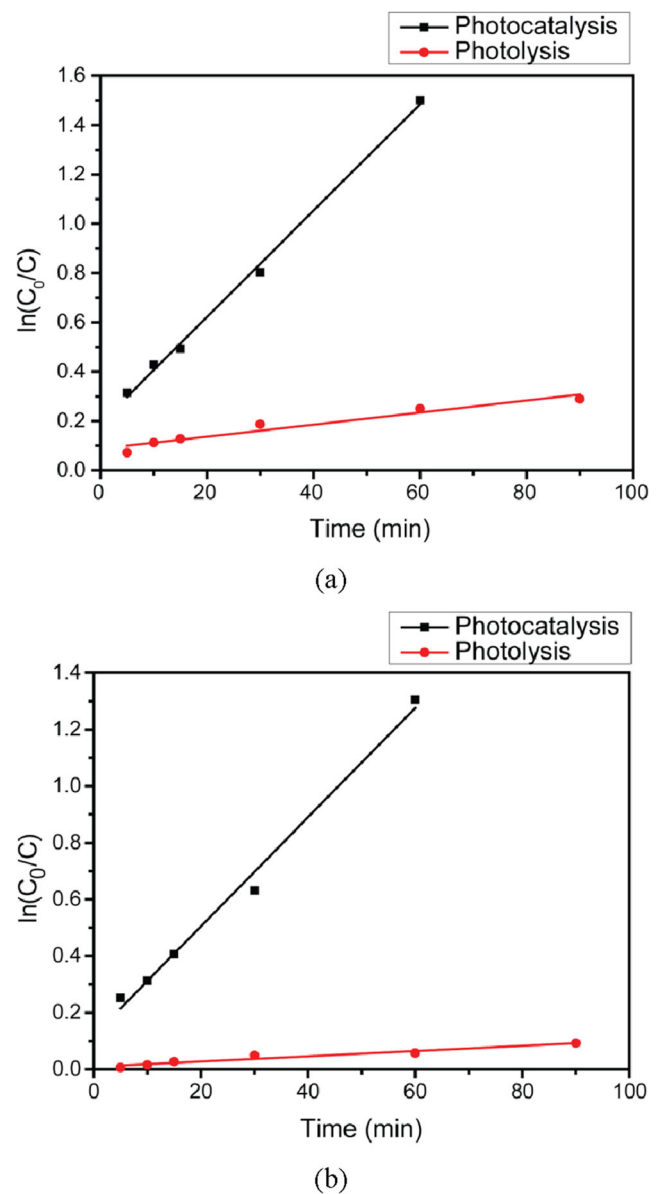


Fig. 11 Kinetic study of the photocatalysis and photolysis processes in the color removal of NB (a) and NY (b) dyes, experimental conditions: Pal-Ti30 composite, pH 2, potency of 18 W and dye concentration 10 mg/L

Table 11 Values of the correlation coefficient (R^2) and apparent reaction rate constant (K_{app}) for NB and NY photolysis and photocatalysis

	Dye	R^2	K_{app} (min^{-1})
Photolysis	NB	0.9416	0.0025
	NY	0.9420	0.0009
Photocatalysis	NB	0.9972	0.0216
	NY	0.9912	0.0193

Total organic carbon (TOC) and analysis of degradation by-products

Figure 12 shows the percentage results of total organic carbon—TOC for the analysis of dye samples after photocatalysis with the use of the Pal-Ti30 composite for 90 min, under UV-C radiation with the power of 18 W. The results obtained after color removal of the dyes NB and NY are compared with the starting solutions of initial concentration 10 mg/L.

The results of the TOC showed that in a time of 90 min, removals of 61.7% and 58.06% of the initial organic matter were obtained for the dyes NB and NY, respectively. This shows that there was a process of mineralization of most of the dye molecules when submitted to the photocatalysis process. As can be seen in Figure 12, even with the removal of 100% of the coloring of both dyes, there is still a percentage of organic matter that corresponds to 38.30% and 41.94% for NB and NY, respectively. These results possibly correspond to intermediates in the degradation process of both dyes.

As in the present work, other studies found in the literature reinforce the effectiveness of titanium dioxide, supported in different matrices, in the photocatalytic degradation of complex pollutants (Rtimi et al. 2015; Azzaz et al. 2018; Zeghioud et al. 2018, 2019). For example, Zeghioud et al. (2019) investigated the photocatalytic degradation of three antibiotics in mono, binary and tertiary systems, using TiO₂ supported on cellulosic paper as a catalyst. The degradation efficiency was higher in mono systems, when compared to the results obtained with binary and ternary systems. One of the antibiotics studied, oxalonic oxide, reached a mineralization rate of 65.4% in a monocomposite system, a result similar to that found in the present work. However, in general, the degradation of pollutants occurred in a longer time, approximately 4 h.

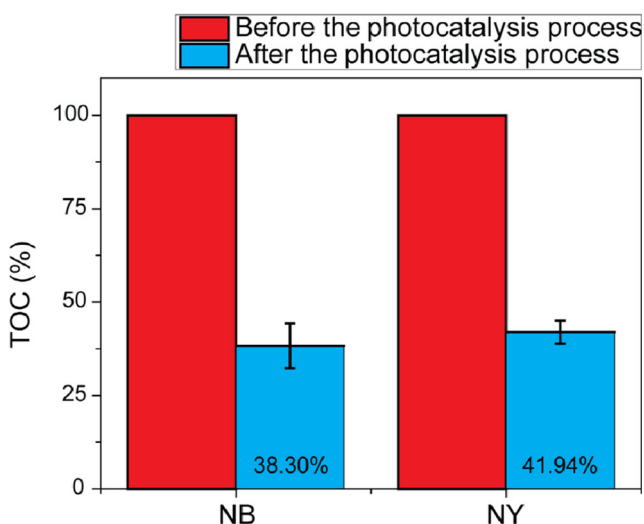


Fig. 12 TOC analysis for NB and NY dyes before and after photocatalysis, experimental conditions: PAL-Ti30 composite, pH 2, 18 W potency and 10 mg/L dye concentration

However, it can be inferred that the catalyst used in this work has a certain advantage in terms of time, where it was possible to remove 100% of the color of the effluents containing the dyes, with a considerable mineralization index, in just 90 min. Such success can be explained by the use of palygorskite as support, a clay mineral that has a high density of silanol groups on the surface. Such groups interact with groups present in dye molecules, facilitating the initial adsorption process and catalyst contact with the pollutant. In addition, the semiconductor will be better dispersed on the surface of the support, preventing agglomeration of particles and, consequently, decreasing its efficiency (Mu and Wang 2016; Yang et al. 2018; Damasceno Junior et al. 2020c, b).

In order to qualitatively identify the by-products formed in the present study, CG-EM analyzes of the solutions generated after the 90-min tests of the photocatalytic process of the studied dyes were performed. In Figures 13b and 14b, the mass spectra obtained in the tests performed are exposed.

To identify possible by-products, the spectral standards contained in the National Institute of Standards and Technology Library (NIST) were used as a comparison. As a result, the presence of aliphatic amide compounds and esters derived from phthalic acid was identified, as shown in the chromatogram and mass spectra shown in the figures below (Figures 13 and 14). Therefore, from the results of TOC and gas chromatography, it can be inferred that the photodegradation process provided a mineralization of approximately 60% for both dyes, with the remainder of the percentage of organic carbon corresponding to complex by-products of degradation. The results can be considered promising, since, in just 90 min of treatment, it was possible to obtain a significant mineralization rate. Possibly, with longer photodegradation times, it would be possible to achieve 89 higher rates of mineralization and/or the conversion of complex by-products into smaller molecules; however, the cost of the process would become higher.

In studies carried out with seven commercial dyes, containing azo group, carried out by Tanaka et al. (2000) (Tanaka et al. 2000), it was observed that after the photocatalysis process using the TiO₂ semiconductor, the main intermediates identified were aromatic amines and phenolic compounds and that these phenolic compounds are intermediates for the photocatalytic degradation of aromatic compounds. In addition, other compounds were identified that were organic acids, the main ones being formic acid and acetic acid. These results are also observed by Rocha et al. (2012) (Rocha et al. 2012) and Rocha et al. (2014) (Rocha et al. 2014), who using electrochemical methods, in a prolonged test, observed in the oxidation of NB and NY, the formation of by-products such as acetic, formic and oxalic acid.

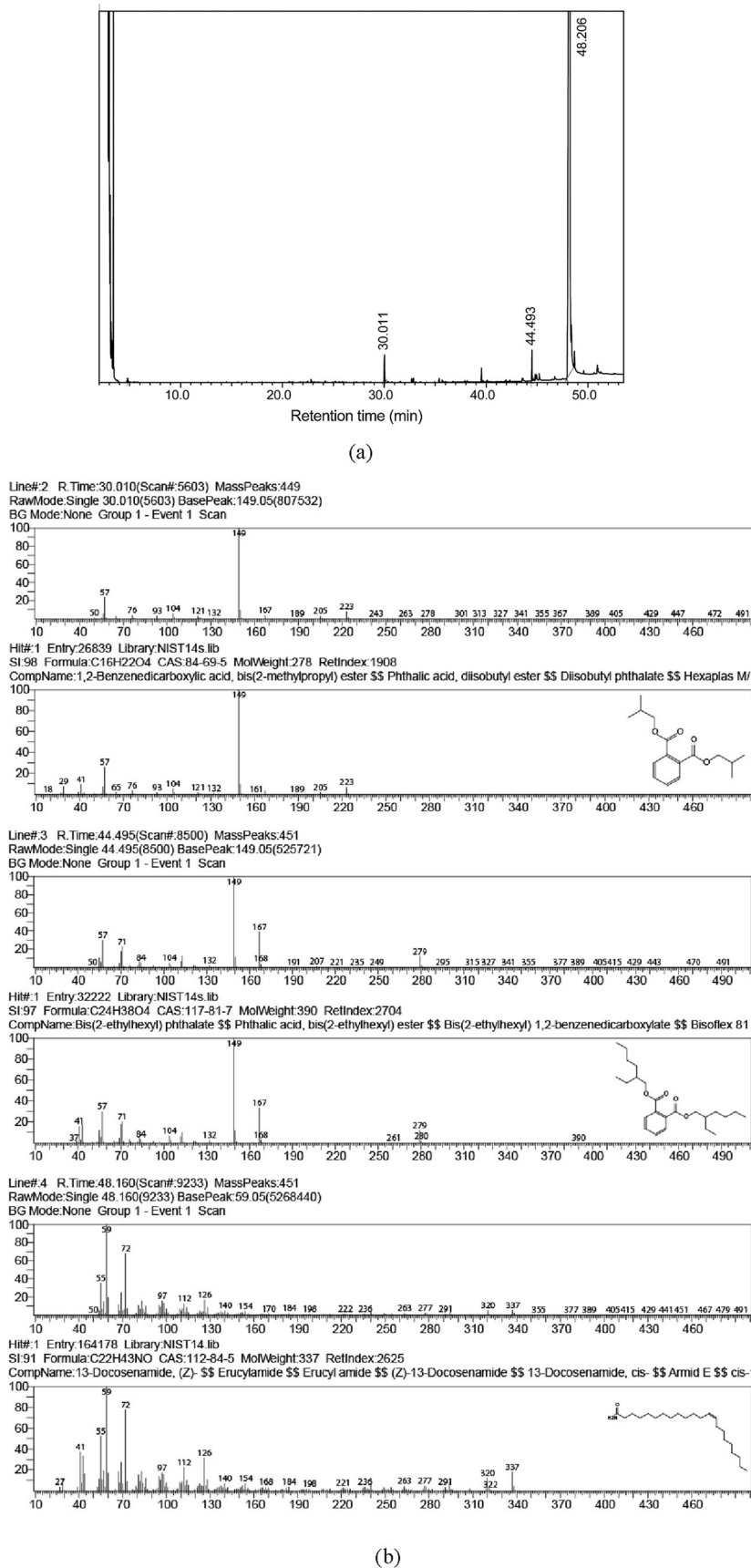
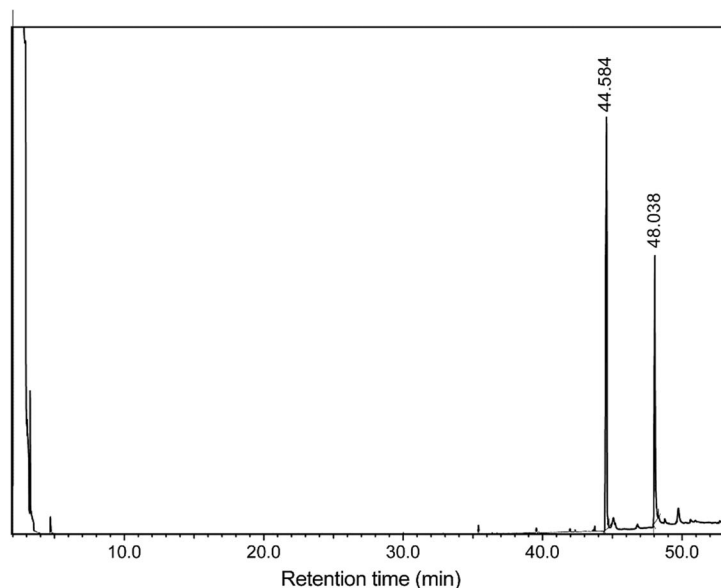
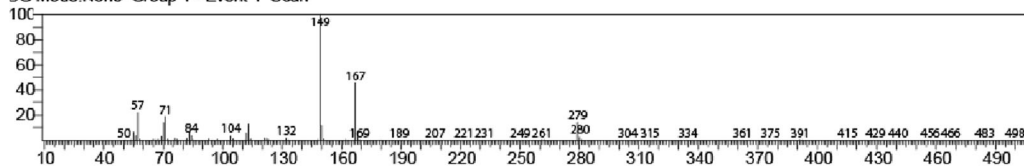


Fig. 13 (a) Chromatogram and (b) mass spectra of the by-products identified for the NB sample

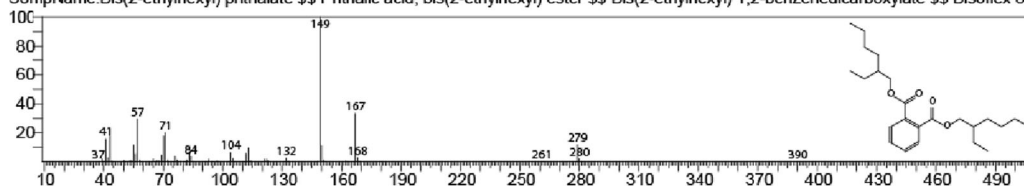


(a)

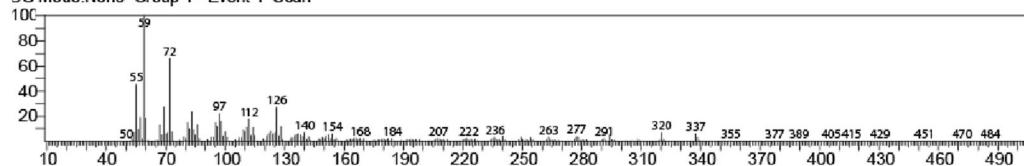
Line#1 R.Time:44.550(Scan#8511) MassPeaks:
RawMode:Single 44.550(8511) BasePeak:149.00(316)
BG Mode:None Group 1 - Event 1 Scan



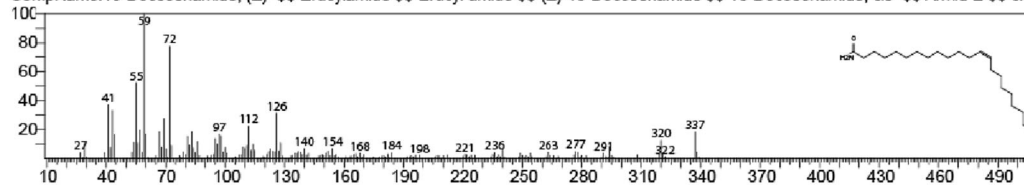
Hit#1 Entry:32222 Library:NIST14s
SI:95 Formula:C24H38O4 CAS:117-81-7 MolWeight:390 RetIndex
CompName:Bis(2-ethylhexyl) phthalate \$\$ Phthalic acid, bis(2-ethylhexyl) ester \$\$ Bis(2-ethylhexyl) 1,2-benzenedicarboxylate \$\$ Bisoflex 81



Line#2 R.Time:48.040(Scan#9209) MassPeaks:
RawMode:Single 48.040(9209) BasePeak:59.05(85)
BG Mode:None Group 1 - Event 1 Scan



Hit#1 Entry:164178 Library:NIST14.lib
SI:94 Formula:C22H43NO CAS:112-84-5 MolWeight:337 RetIndex
CompName:13-Docosamide, (Z)- \$\$ Erucylamide \$\$ Erucyl amide \$\$ (Z)-13-Docosamide \$\$ 13-Docosamide, cis- \$\$ Armid E \$\$ cis-



(b)

Fig. 14 (a) Chromatogram and (b) mass spectra of the by-products identified for the NY sample

Table 12 Energy consumption and cost of treatment for individual photocatalysis of NB and NY dyes (10 mg/L)

Time (h)	Energy consumption (kWh/dm ³)	Energy cost (R\$/kWh)	Final cost (R\$/dm ³)
1.5	0.1350	0.6628	0.0895

Cost of photocatalysis treatment

The cost of treatment is a very important factor in determining whether the method implemented for photodegradation of NB and NY dyes is economically viable. The results were obtained according to the values provided by the National Electric Energy Agency of Brazil—ANEEL.

The calculation of energy consumption followed Eq. 7 (Silva et al. 2019).

$EC = IVt/1000V_s$ (7) where EC is the energy cost, I is the current (A), V is the voltage applied to the UV lamps (Voltz), t is the time required for dye decoloration and V_s is the solution volume (dm³) used in the photocatalytic test.

Table 12 shows the values obtained for the energy cost and the final cost in the photocatalysis process in a time of 90 min (1.5 h). The amounts paid in reais for final consumption were obtained by multiplying the energy cost (R\$/kWh) and energy consumption (kWh/dm³).

The result obtained corresponds to the amount spent for each 1 dm³ of effluent treated by photocatalysis in a time of 1.5 h of activity under UV-C light. The value corresponding to 1.5 h of photocatalysis is 8.95 cents, showing how much the proposed treatment is viable and of low cost.

Although the costs are similar to those reported in tests performed via electrochemical processes (Rocha et al. 2012, 2014; Fernandes Rêgo et al. 2014), it can be observed that in a matter of discoloration time, treatments via photocatalysis stand out since 100% color removal results were obtained from the studied dyes in a short treatment time. In addition, it is worth mentioning that the catalyst used in the photocatalytic treatment had low-cost material precursors, which makes the technique very promising in removing contaminants (Szczepanik 2017).

Conclusions

The present work showed that the palygorskita-TiO₂ composite was synthesized in a simple way, and its performance in the photocatalytic activity showed that this catalyst is an excellent candidate for photodegradation of reactive dyes of the azo type, as is the case of industrial dyes NB and NY. The

techniques used to characterize the synthesized composites showed the incorporation of TiO₂ in Pal. The use of factorial design was of paramount importance for the optimization of the results of discoloration by photocatalytic activity of the dyes. The results of total organic carbon (TOC) showed a mineralization of approximately 60% for both dyes, and the degradation by-products were identified by gas chromatography. For the final cost of treatment, photodegradation tests had viable results in efficiency and economy.

Acknowledgements To Petrobras, IQ-UFRN, DEMAT-UFRN, DEQ-UFRN, NUPLAM-UFRN, LASID-UFRN and LABPEMOL-UFRN for the instrumental support. At NUPPRAR-UFRN and Bentonit União do Nordeste for the supply of inputs.

Author contribution Conceptualization: all authors; methodology: M.L.M.A., R.V.B., L.M.S., E.F.D.; formal analysis and investigation: M.L.M.A., E.D.J., J.M.F.A., I.N.S.; writing—original draft preparation: M.L.M.A., E.D.J.; writing—review and editing: N.S.F., C.A.M.H.; resources: M.L.M.A., E.D.J., R.V.B., L.M.S., N.S.F., C.A.M.H.; supervision: N.S.F., C.A.M.H.

Funding To CNPq—Conselho Nacional de Desenvolvimento Científico e Tecnológico for the financial support.

Availability of data and materials Not applicable.

Declarations

Ethics approval and consent to participate Not applicable.

Consent for publication Not applicable.

Competing interests The authors declare no competing interests.

References

- Al-Mamun MR, Kader S, Islam MS, Khan MZH (2019) Photocatalytic activity improvement and application of UV-TiO₂ photocatalysis in textile wastewater treatment: A review. *J Environ Chem Eng* 7: 103248
- Awad AM, Shaikh SMR, Jalab R, Gulied MH, Nasser MS, Benamor A, Adham S (2019) Adsorption of organic pollutants by natural and modified clays: a comprehensive review. *Sep Purif Technol* 228: 115719
- Azari A, Nabizadeh R, Nasser S, Mahvi AH, Mesdaghinia AR (2020) Comprehensive systematic review and meta-analysis of dyes adsorption by carbon-based adsorbent materials: classification and analysis of last decade studies. *Chemosphere* 250:126238
- Azzaz AA, Assadi AA, Jellali S, Bouzaza A, Wolbert D, Rtimi S, Bousselmi L (2018) Discoloration of simulated textile effluent in continuous photoreactor using immobilized titanium dioxide: effect of zinc and sodium chloride. *J Photochem Photobiol A Chem* 358: 111–120. <https://doi.org/10.1016/j.jphotochem.2018.01.032>
- Baccaro A, Cordon L, Nishimura F, Gutz I (2019) Fotocatálise Mediada Por TiO₂ no estado nanoparticulado: revisão da reatividade pelo

- conceito de traps e algumas aplicações em química analítica. *Quim Nova* 42:329–345. <https://doi.org/10.21577/0100-4042.20170332>
- Bamba D, Coulibaly M, Robert D (2017) Nitrogen-containing organic compounds: origins, toxicity and conditions of their photocatalytic mineralization over TiO₂. *Sci Total Environ* 580:1489–1504
- Barros Neto B, Scarmino IS, Bruns RE (2010) Como fazer experimentos: pesquisa e desenvolvimento na indústria. Bookman
- Bilal M, Adeel M, Rasheed T, et al (2019) Emerging contaminants of high concern and their enzyme-assisted biodegradation—a review. *Environ Int* 124:336–353
- Bouna L, Rhouta B, Amjoud M, Maury F, Lafont MC, Jada A, Senocq F, Daoudi L (2011) Synthesis, characterization and photocatalytic activity of TiO₂ supported natural palygorskite microfibers. *Appl Clay Sci* 52:301–311. <https://doi.org/10.1016/j.clay.2011.03.009>
- Brillas E, Martínez-Huitle CA (2015) Decontamination of wastewaters containing synthetic organic dyes by electrochemical methods. An updated review. *Appl Catal B Environ* 166–167:603–643
- Buruga K, Song H, Shang J, Bolan N, Jagannathan TK, Kim KH (2019) A review on functional polymer-clay based nanocomposite membranes for treatment of water. *J Hazard Mater* 379:120584. <https://doi.org/10.1016/j.jhazmat.2019.04.067>
- Chang PH, Li Z, Yu TL, Munkhbayer S, Kuo TH, Hung YC, Jean JS, Lin KH (2009) Sorptive removal of tetracycline from water by palygorskite. *J Hazard Mater* 165:148–155. <https://doi.org/10.1016/j.jhazmat.2008.09.113>
- Chen D, Zhu Q, Zhou F, Deng X, Li F (2012) Synthesis and photocatalytic performances of the TiO₂ pillared montmorillonite. *J Hazard Mater* 235–236:186–193. <https://doi.org/10.1016/j.jhazmat.2012.07.038>
- Chong MN, Jin B, Chow CWK, Saint C (2010) Recent developments in photocatalytic water treatment technology: a review. *Water Res* 44:2997–3027
- Damasceno Junior E, de Almeida JMF, Silva I do N et al (2020a) pH-responsive release system of isoniazid using palygorskite as a nanocarrier. *J Drug Deliv Sci Technol* 55:101399. <https://doi.org/10.1016/j.jddst.2019.101399>
- Damasceno Junior E, De Almeida JMF, Silva IDN et al (2020b) Obtaining and applying nanohybrid palygorskite-rifampicin in the pH-responsive release of the tuberculostatic drug. *Langmuir*. 36:10251–10269. <https://doi.org/10.1021/acs.langmuir.0c01834>
- Damasceno Junior E, Almeida JMF, Silva IDN et al (2020c) pH-responsive release system of isoniazid using palygorskite as a nanocarrier. *J Drug Deliv Sci Technol* 55:101399. <https://doi.org/10.1016/j.jddst.2019.101399>
- Dos Santos SD, Fernandes CS, Da Costa ACS et al (2013) Characterization of palygorskite clay from Piauí, Brazil and its potential use as excipient for solid dosage forms containing anti-tuberculosis drugs. *J Therm Anal Calorim* 113:551–558. <https://doi.org/10.1007/s10973-013-3291-0>
- Fernades Rêgo FE, Sales Solano AM, Da Costa Soares IC et al (2014) Application of electro-Fenton process as alternative for degradation of Novacron Blue dye. *J Environ Chem Eng* 2:875–880. <https://doi.org/10.1016/j.jece.2014.02.017>
- Gouvêa D, Murad BBS (2001) Influência das características ácido-básicas da superfície dos óxidos na estabilidade de suspensões cerâmicas de Al₂O₃ ou SnO₂ com dispersantes comerciais. *Cerâmica* 47:51–56
- Hassan MM, Carr CM (2018) A critical review on recent advancements of the removal of reactive dyes from dyehouse effluent by ion-exchange adsorbents. *Chemosphere* 209:201–219
- Hassani A, Soltani RDC, Karaca S, Khataee A (2015) Preparation of montmorillonite-alginate nanobiocomposite for adsorption of a textile dye in aqueous phase: isotherm, kinetic and experimental design approaches. *J Ind Eng Chem* 21:1197–1207. <https://doi.org/10.1016/j.jiec.2014.05.034>
- Hosseini SN, Borghei SM, Vossoughi M, Taghavinia N (2007) Immobilization of TiO₂ on perlite granules for photocatalytic degradation of phenol. *Appl Catal B Environ* 74:53–62. <https://doi.org/10.1016/j.apcatb.2006.12.015>
- Kuang M, Zhang J, Wang W, Chen J, Cao Y, Wang J, Ji Z (2019) Ternary Ag-deposited TiO₂/palygorskite composites with synergistic effect for enhanced photocatalytic activity. *Solid State Sci* 97:106015. <https://doi.org/10.1016/j.solidstatesciences.2019.106015>
- Liu W, Du T, Ru Q et al (2018) Preparation of attapulgite/TiO₂/graphene composite and its application for the photocatalytic degradation of chlorotetracycline. *Nanotechnol Environ Eng* 3:5. <https://doi.org/10.1007/s41204-018-0035-1>
- Matilainen A, Sillanpää M (2010) Removal of natural organic matter from drinking water by advanced oxidation processes. *Chemosphere* 80:351–365
- Mishra A, Mehta A, Basu S (2018) Clay supported TiO₂ nanoparticles for photocatalytic degradation of environmental pollutants: a review. *J Environ Chem Eng* 6:6088–6107
- Moraes JDD, Bertolino SRA, Cuffini SL, Ducart DF, Bretzke PE, Leonardi GR (2017) Clay minerals: properties and applications to dermocosmetic products and perspectives of natural raw materials for therapeutic purposes—a review. *Int J Pharm* 534:213–219
- Mu B, Wang A (2016) Adsorption of dyes onto palygorskite and its composites: a review. *J Environ Chem Eng* 4:1274–1294
- Nguyen CH, Juang RS (2019) Efficient removal of cationic dyes from water by a combined adsorption-photocatalysis process using platinum-doped titanate nanomaterials. *J Taiwan Inst Chem Eng* 99:166–179. <https://doi.org/10.1016/j.jtice.2019.03.017>
- Nguyen CH, Tran HN, Fu CC, Lu YT, Juang RS (2020) Roles of adsorption and photocatalysis in removing organic pollutants from water by activated carbon-supported titania composites: kinetic aspects. *J Taiwan Inst Chem Eng* 109:51–61. <https://doi.org/10.1016/j.jtice.2020.02.019>
- Papoulis D, Komarneni S, Nikolopoulou A, Tsohis-Katagas P, Panagiotaras D, Kacandes HG, Zhang P, Yin S, Sato T, Katsuki H (2010) Palygorskite- and halloysite-TiO₂ nanocomposites: synthesis and photocatalytic activity. *Appl Clay Sci* 50:118–124. <https://doi.org/10.1016/j.clay.2010.07.013>
- Papoulis D, Komarneni S, Panagiotaras D, Nikolopoulou A, Li H, Yin S, Tsugio S, Katsuki H (2013) Palygorskite-TiO₂ nanocomposites: Part 1 Synthesis and characterization. *Appl Clay Sci* 83–84:191–197. <https://doi.org/10.1016/j.clay.2013.09.003>
- Queiroz MTA, Queiroz CA, Alvim LB, Sabará MG, Leão MMD, Amorim CC (2019) Reestruturação na forma do tratamento de efluentes têxteis: uma proposta embasada em fundamentos teóricos. *Gestão & Produção* 26:e1149. <https://doi.org/10.1590/0104-530x1149-19>
- Reza KM, Kumy A, Gulshan F (2017) Parameters affecting the photocatalytic degradation of dyes using TiO₂: a review. *Appl Water Sci* 7:1569–1578. <https://doi.org/10.1007/s13201-015-0367-y>
- Rocha JHB, Solano AMS, Fernandes NS, da Silva DR, Peralta-Hernandez JM, Martínez-Huitle CA (2012) Electrochemical degradation of Remazol Red BR and Novacron Blue C-D dyes using diamond electrode. *Electrocatalysis*. 3:1–12. <https://doi.org/10.1007/s12678-011-0070-1>
- Rocha JHB, Gomes MMS, Dos Santos EV et al (2014) Electrochemical degradation of Novacron Yellow C-RG using boron-doped diamond and platinum anodes: direct and indirect oxidation. *Electrochim Acta* 140:419–426. <https://doi.org/10.1016/j.electacta.2014.06.030>
- Rodrigues MI, Iemma AF (2014) *Experimental Design and Process Optimization* (1st ed.). CRC Press. <https://doi.org/10.1201/b17848>
- Rtimi S, Pulgarin C, Sanjines R, Kiwi J (2015) Kinetics and mechanism for transparent polyethylene-TiO₂ films mediated self-cleaning leading to MB dye discoloration under sunlight irradiation. *Appl*

- Catal B Environ 162:236–244. <https://doi.org/10.1016/j.apcatb.2014.05.039>
- Shi Y, Zhang Q, Zhu X et al (2017) Palygorskite supported BiVO₄ photocatalyst for tetracycline hydrochloride removal. *Appl Clay Sci* 137:249–258. <https://doi.org/10.1016/j.clay.2016.12.035>
- Silva IDN, Damasceno Júnior E, Almeida JMFD et al (2019) Experimental design for optimization of the photocatalytic degradation process of the remazol red dye by the TiO₂ expanded perlite composite. *Environ Technol* 42:1493–1505. <https://doi.org/10.1080/09593330.2019.1672794>
- Stathatos E, Papoulis D, Aggelopoulos CA, Panagiotaras D, Nikolopoulou A (2012) TiO₂/palygorskite composite nanocrystalline films prepared by surfactant templating route: synergistic effect to the photocatalytic degradation of an azo-dye in water. *J Hazard Mater* 211–212:68–76. <https://doi.org/10.1016/j.jhazmat.2011.11.055>
- Szczepanik B (2017) Photocatalytic degradation of organic contaminants over clay-TiO₂ nanocomposites: a review. *Appl Clay Sci* 141:227–239
- Tanaka K, Padermpole K, Hisanaga T (2000) Photocatalytic degradation of commercial azo dyes. *Water Res* 34:327–333. [https://doi.org/10.1016/S0043-1354\(99\)00093-7](https://doi.org/10.1016/S0043-1354(99)00093-7)
- Tomul F, Arslan Y, Başoğlu FT, Babuçcuoğlu Y, Tran HN (2019) Efficient removal of anti-inflammatory from solution by Fe-containing activated carbon: adsorption kinetics, isotherms, and thermodynamics. *J Environ Manag* 238:296–306. <https://doi.org/10.1016/j.jenvman.2019.02.088>
- Xavier KCM, Silva Filho EC, Santos MSF, Santos MRMC, da Luz AB (2012) Caracterização mineralógica, morfológica e de superfície da atapulgita de Guadalupe-Pi. *Holos* 5:60–70. <https://doi.org/10.15628/holos.2012.1111>
- Xu J, Gao J, Liu Y, Li Q, Wang L (2017) Fabrication of In₂O₃/Co₃O₄-palygorskite composites by the pyrolysis of In/Co-MOFs for efficient degradation of methylene blue and tetracycline. *Mater Res Bull* 91:1–8. <https://doi.org/10.1016/j.materresbull.2017.03.018>
- Yagub MT, Sen TK, Afroze S, Ang HM (2014) Dye and its removal from aqueous solution by adsorption: a review. *Adv Colloid Interf Sci* 209:172–184
- Yang R, Li D, Li A, Yang H (2018) Adsorption properties and mechanisms of palygorskite for removal of various ionic dyes from water. *Appl Clay Sci* 151:20–28. <https://doi.org/10.1016/j.clay.2017.10.016>
- Zeghioud H, Assadi AA, Khellaf N, Djelal H, Amrane A, Rtimi S (2018) Reactive species monitoring and their contribution for removal of textile effluent with photocatalysis under UV and visible lights: dynamics and mechanism. *J Photochem Photobiol A Chem* 365:94–102. <https://doi.org/10.1016/j.jphotochem.2018.07.031>
- Zeghioud H, Kamagate M, Coulibaly LS, Rtimi S, Assadi AA (2019) Photocatalytic degradation of binary and ternary mixtures of antibiotics: reactive species investigation in pilot scale. *Chem Eng Res Des* 144:300–309. <https://doi.org/10.1016/j.cherd.2019.02.015>
- Zhang T, Li Z, Wang W, Wang Y, Gao B, Wang Z (2019) Enhanced antifouling and antimicrobial thin film nanocomposite membranes with incorporation of palygorskite/titanium dioxide hybrid material. *J Colloid Interface Sci* 537:1–10. <https://doi.org/10.1016/j.jcis.2018.10.092>
- Zhang H, Wang J, Xie K, Pei L, Hou A (2020) Synthesis of novel green reactive dyes and relationship between their structures and printing properties. *Dyes Pigments* 174:108079. <https://doi.org/10.1016/j.dyepig.2019.108079>

Publisher's note Springer Nature remains neutral with regard to jurisdictional claims in published maps and institutional affiliations.